

# ELECTRON CLOUD EFFECTS IN PRESENT AND FUTURE HIGH INTENSITY HADRON MACHINES

M. Blaskiewicz\*<sup>†</sup> BNL, Upton NY 11973, USA

## 1 INTRODUCTION

Electron cloud effects have manifested in several Hadron Machines. Table 1 lists basic machine parameters of past and present hadron machines where electron clouds have influenced operations. This instability has also been seen in the AGS Booster[15], but under extreme conditions. Table 2 lists high intensity proton machines that are under construction. The goal of the present work is to take what is known about electron cloud problems in current machines, mainly the LANL PSR, and attempt to extrapolate to the new machines.

## 2 FORMATION OF THE ELECTRON CLOUD

Electron clouds created by gas stripping [18, 19, 20, 21], foil scattering [6, 22, 7], or losses are present in all accelerators, to some extent. For problems to occur the initial seed distribution needs to be amplified <sup>1</sup>. For short

\*blaskiewicz@bnl.gov

<sup>†</sup> Work performed under contract number #DE-AC05-00OR2275 with the auspices of the U.S. Department of Energy

<sup>1</sup>The BINP PSR, which used high gas density, is a notable exception

	$I_{peak}$	$\frac{\sigma_f}{f}$	$\sigma_{\perp}$	$KE$	$b$	$Q_{\beta}$
	(A)	$10^{-5}$	(mm)	(GeV)	(mm)	
BINP PSR 1-3	0.5	1300	2.5	0.001	40	0.7
CERN ISR 4,5	20	14	2	30	35	8.9
LANL PSR 6-8	70	63	7.6	0.787	50	2.2
CERN SPS 9	7	0.26	2.5	26	23	26.6
CERN PS 10,11	7	1.9	6.3	26	35	6.2
BNL RHIC 12-14	2	0.4	2	11A	30	28.2

Table 1: Basic machine parameters for past and existing hadron machines with electron clouds. For RHIC the ion species is gold, with a kinetic energy of 11GeV/nucleon. All the others are proton machines.

	ORNL SNS[16]	J-PARC 3 GeV[17]	J-PARC 50 GeV[17]
$I_{peak}$ (A)	80	20 - 38	38 - 196
$\frac{\sigma_f}{f}$ ( $10^{-5}$ )	55	590 - 32	41 - 0.33
$\sigma_{\perp}$ (mm)	14	19 - 12	11 - 5
$KE$ (GeV)	1	0.375 - 3	3 - 50
$b$ (mm)	100	125	65
$Q_{\beta}$	6.3	4.2	22.2

Table 2: Basic machine parameters for high intensity proton machines under construction. For the J-PARC machines parameters are labeled as injection - extraction .

bunches the process has been considered by many authors [18, 19, 20, 21]. For the LANL PSR, and the machines in Table 2, the bunches are long and an electron trapped within the beam performs many transverse oscillations during a single bunch passage [23]. Fig. 1 shows a simulation for typical PSR parameters. If the electron line charge density,  $\lambda_e$  (units of Coulombs/meter) is small compared with the proton line charge density,  $\lambda_p$  then a fairly accurate expression for the strike energy can found [16]

$$E_{strike} = -\frac{\pi m_e c^2}{2} \left(\frac{b}{c}\right)^2 \frac{d\omega_e}{dt}, \quad (1)$$

where  $b$  is the beam pipe radius,  $c$  is the speed of light, and the instantaneous electron oscillation frequency is

$$\omega_e(t) = \sqrt{\frac{e\lambda_p(t)}{2\pi\epsilon_0 m_e (\sigma^2 + 2b^2/\pi)}}, \quad (2)$$

with  $\sigma$  the rms beam radius. The strike energy is positive on the trailing edge of the bunch ( $\dot{\omega}_e < 0$ ) and equation (1) is valid only when the electron frequency does not have a large fractional change per period,  $|\dot{\omega}_e| \ll \omega_e^2$ . From the PSR simulation the electron has an energy of 45 eV for the first wall strike, while equation (1) predicts 55 eV. Typical numbers for ISIS give  $E_{strike} \lesssim 10$  eV.

When an electron strikes a surface it can be reflected, rediffused or stopped<sup>2</sup>. During this process another electron may gain enough energy to leave the surface. A useful experimental measure is the secondary emission yield: the ratio of the total number of electrons leaving the surface to the total number incident upon the surface. Figure 2 shows measurements of secondary yield for titanium nitride coated stainless steel with normally incident electrons.

<sup>2</sup>This is a phemonenolgical, classical picture

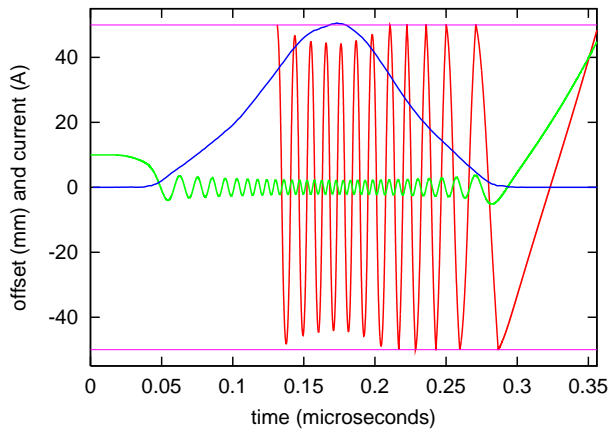


Figure 1: Proton beam current (blue) and positions for captured (green) and loss created (red) electrons. The beam pipe radius is 50 mm (violet).

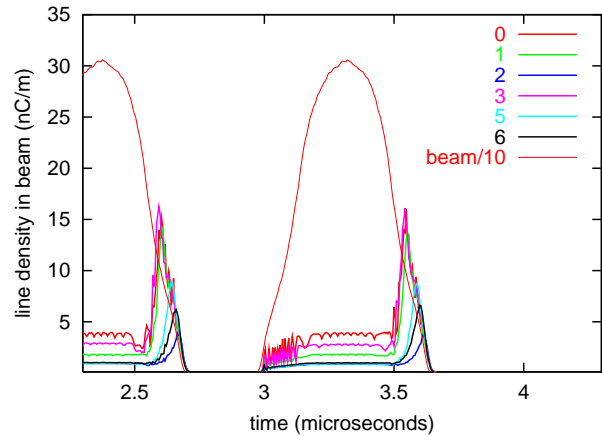


Figure 3: SNS line charge densities for the beam and electron cloud within  $r = \sigma$  for each of the six secondary yield curves in Fig. 2.

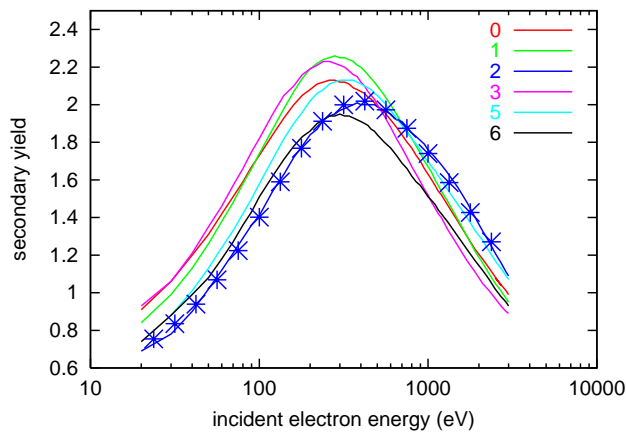


Figure 2: Secondary emission yield for titanium nitride coated stainless steel from similarly manufactured samples. The samples were manufactured by P.He and H.C. Hseuh of the BNL vacuum group. The measurements were performed by B. Henrist of the CERN vacuum group. The surfaces have not been baked or conditioned in any way. The solid lines are data and the markers are a fit of the CSEC model to the blue curve. Of all the fits, the one shown had the largest rms deviation from the data, 0.025.

The data in Figure 2 have been fitted using a phenomenological model and that model was subsequently used in a simulation of electron cloud formation for the SNS. This cylindrically symmetric electron cloud code (CSEC) and its benchmarking against M. Furman's positron instability code (POSINST [25]) are described in [16]. Figure 3 shows the proton line density and the electron line density within one  $\sigma$  of the beam axis. The primary electrons were estimated assuming 1% of the beam was lost over 1000 turns and that 20 electrons were generated by each lost proton [24]. The electrons create a focusing lens, which travels with the beam. For SNS with 15 nC/m of electrons in the beam the electrons give a tune shift  $\approx +0.05$ .

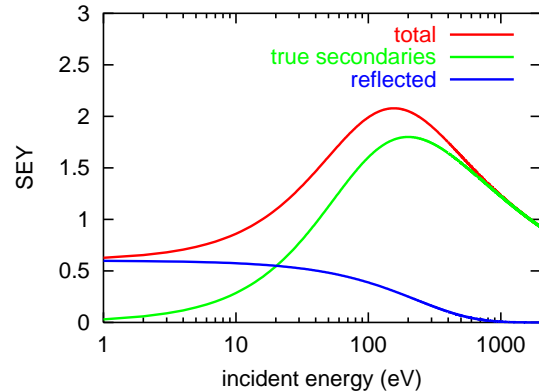


Figure 4: Secondary yield curve for stainless steel. Note the significant reflections at low energy.

Figure 4 shows a reasonable secondary yield curve for clean stainless steel. Taking this secondary yield, 20 electrons per lost proton, 0.1% beam loss over 2000 turns, and parameters for the J-PARC 3 GeV rapid cycling synchrotron [17] yields Figure 5. The peak electron line density from these CSEC simulations corresponds to an instantaneous neutralization of 1.2% at extraction. Increasing the electron generation rate by a factor of 10 changed the results by less than 10%. The electron clouds pictured in Figures 3 and 5 evolve as the beam passes and result in a considerable electron flux to the wall. For Figure 3 the net charge per turn varies between 40 and 700 pC/cm<sup>2</sup>/turn with electrons in excess of 100 eV depositing between 10 and 50 pC/cm<sup>2</sup>/turn. For the J-PARC simulations the total charge per turn is 45 and 110 pC/cm<sup>2</sup>/turn for injection and extraction, respectively. Only about 1% of these electrons have a strike energy greater than 100 eV.

These electrons striking the wall will desorb gas molecules and can cause the pressure to rise [20, 26, 27]. For machines with a large duty cycle a dramatic pressure rise can result from a very modest electron flux. Over time,

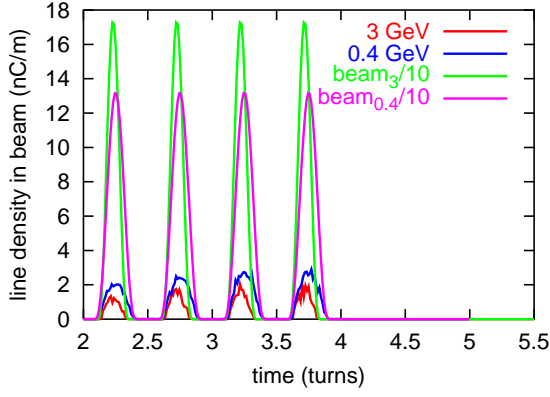


Figure 5: Line charge densities for the beam and electron cloud within  $r = \sigma$  for the J-PARC 3 GeV RCS, using the secondary yield curve in Fig. 4.

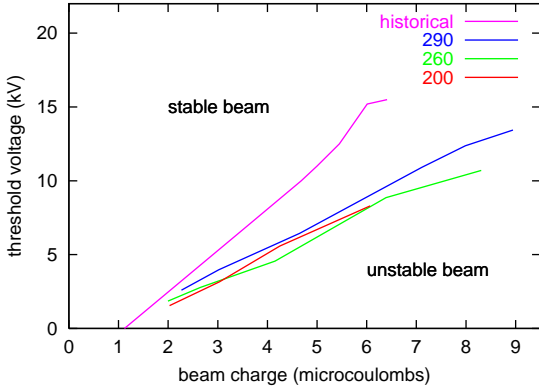


Figure 6: Threshold RF voltage versus beam intensity for PSR, courtesy R.J. Macek. The threshold RF voltage is the smallest RF voltage for which the beam is stable. The historical curve represents the situation before the direct  $H^-$  injection upgrade and the extended run during 2001. Threshold curves near the end of the 2001 run for injected bunch lengths of 200, 260, and 290 ns are shown for comparison.

the adsorbed gas will be exhausted. Also, the electrons striking the wall eventually reduce the secondary yield. The desorbed gas places requirements on the vacuum system. Significant reduction in the secondary yield requires a net electron dose of order  $0.1 \text{ C/cm}^2$  [28, 29]. If the SNS beam is stable under the conditions shown in Figure 3, this conditioning will take about a week of running time. Scaling to J-PARC parameters, a few weeks of running time are needed for conditioning. The question at hand is whether the beam will be stable at sufficiently high intensity for conditioning to occur.

### 3 EC INSTABILITY

The electron cloud instability in the LANL PSR has been well documented [6, 8, 30, 31, 32, 33, 16]. Figure 6 shows the threshold RF voltage as a function of beam current for

different epochs and bunch lengths. When the instability occurs, the observed oscillation frequency agrees with the calculated electron oscillation frequency [30]. The threshold is quite sharp [16], so one expects that a linearized calculation should provide adequate threshold estimates.

Bunched beam stability estimates based on the linearized Vlasov equation are a natural starting point. Early treatments considered positron bunches [34, 35], and techniques developed for the transverse mode coupling instability [36] yielded results which agreed with simulations [37, 38, 34]. For high intensity proton machines the bunches are long and electrons perform many oscillations as the bunch passes. Traditional techniques require matrices with millions of elements and are a significant computational challenge. An alternate technique, which models the RF system using a barrier bucket, yields much smaller matrices [16]. Since the bunch is square the electron oscillation frequency is constant within the bunch

$$\omega_e = \omega_0 Q_e = \sqrt{\frac{e\lambda_p}{2\pi\epsilon_0 m_e a^2}},$$

where  $\omega_0$  is the angular revolution frequency and  $a$  is the beam radius. The strength of the electron cloud interaction is determined by the parameter

$$Q_p^2 = \frac{e\lambda_e}{2\pi\epsilon_0 \omega_0^2 \gamma m_p a^2}, \quad (3)$$

where we assume that the cloud has the same radius as the beam<sup>3</sup>. Even though we take the radii to be equal, the proton beam radius varies with the lattice functions. To model this spread we assume the electron response function can be modeled as a parallel LRC resonator with quality factor  $Q_r$ .

Figure 7 compares the output of the bunched beam eigenvalue code with thresholds obtained using the coasting beam dispersion relation [40, 4, 5, 41, 42],

$$1 = \Delta Q_0 \int \frac{dv \rho(v)}{\Delta Q + \Delta Q_{sc} - v Q_e}, \quad (4)$$

where  $v = (\omega - \omega_0)/\omega_0$  is the fractional frequency difference,  $\rho(v)$  is the normalized density with  $\int \rho(v) dv = 1$ ,  $\Delta Q$  is the coherent tune when frequency spread is included, and  $\Delta Q_{sc}$  is the space charge tune shift. The cold beam tune shift is

$$\Delta Q_0 = \Delta Q_{sc} + i \frac{Q_p^2 Q_r}{2Q_\beta}. \quad (5)$$

where  $Q_\beta$  is the betatron tune. The derivation of equation 4 assumes  $\Delta Q \ll Q_\beta$  and  $Q_r \ll Q_e$ . Taking lattice functions for PSR and SNS, calculating the variation in  $\omega_e$  for an elliptical (KV) beam, and equating equivalent widths of the resistive transfer function; one finds  $Q_r \approx 3$ .

<sup>3</sup>Notice that  $Q_p$  is the betatron tune the protons would have in the absence of other focussing forces.

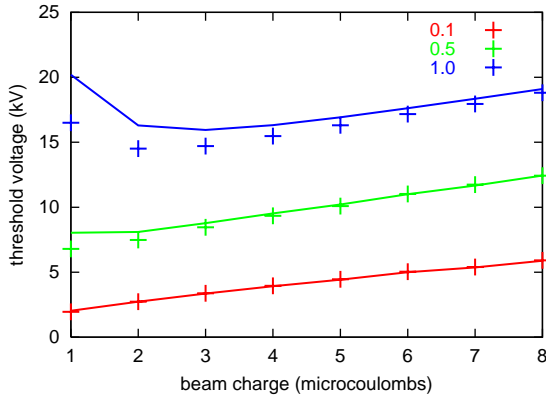


Figure 7: Threshold voltage versus bunch charge for the PSR parameter regime. The symbols are the thresholds for the bunched beam eigenvalue problem. The solid line is the estimate using the coasting beam dispersion relation, equation (4). The different colors correspond to  $\lambda_e = 1, 0.5,$  and  $0.1$  nC/m.

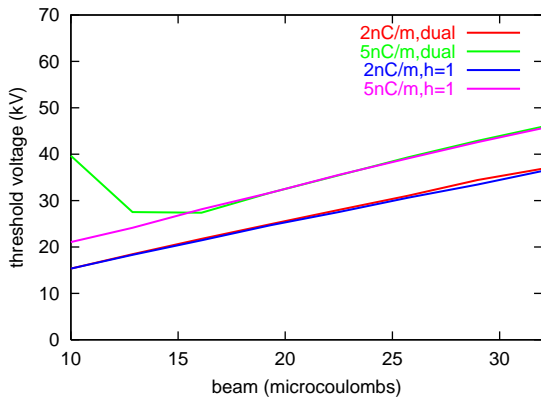


Figure 8: Threshold  $h = 1$  voltage versus bunch charge for SNS. These were done for a dual harmonic RF system, as well as for  $h = 1$  alone. The design  $h = 1$  voltage for SNS is 40 kV.

In [16] threshold voltages were calculated for a variety of beam and cloud parameters. However, the various codes calculated values of  $Q_e$  and  $Q_p$  too large by a factor of  $\sqrt{2}$ . Additionally, the estimates now use the peak beam current, and momentum distributions calculated from a simulation of multi-turn injection. The PSR calculations still give values of threshold voltage that are 3 to 4 times larger than in Fig 6. Results for SNS are shown in Figure 8.

Other hand calculations include centroid models [43, 35], which are known as beam break-up models in the linac community. The basic idea here is to neglect synchrotron oscillations so that one can integrate out the dependence on  $(\omega - \omega_0)/\omega_0$ . The shape of the unstable modes look similar to those observed in PSR but threshold estimates are difficult.

Behavior of the instability well beyond threshold is discussed in [44]. Including the dependence of electron oscillation frequency with electron amplitude reduces the

growth rate of the instability. This is in line with the growth rates observed in PSR, which are significantly slower than those from equation (5).

## 4 SIMULATIONS

Simulations of both coasting [47, 48, 49] and bunched [45, 46, 17, 16] beams have been done. The coasting beam simulations involve a fully 3-dimensional solution to the Vlasov equation, but do not yet include the effects of secondary emission. The bunched beam simulations use approximate equations of motion for the protons and electrons but some include secondary emission and synchrotron oscillations. One key question regards the effect of nonlinear forces. The coasting beam simulations [49, Figs 2 and 3] show that electron cloud instabilities do not exist for cold beams if the beam and cloud densities are low enough. This is well known when there is no spread in the electron bounce frequency, and this frequency is sufficiently far from the nearest, unstable, betatron sideband [40, 5, 15]. However, the simulations in [49] have electron frequency spread. In [16] the inclusion of nonlinear space charge effects led to estimates in better agreement with experimental PSR stability thresholds. In the meantime, the author has done some simulations of the equation

$$\frac{d^2 \mathbf{x}_j}{d\theta^2} + Q_j^2 \mathbf{x}_j = \frac{1}{N} \sum_{k=1}^N \left( \nu \mathbf{x}_k + \alpha \frac{d\mathbf{x}_k}{d\theta} \right) + \frac{C_{sc}}{N} \sum_{k=1}^N \frac{\mathbf{x}_j - \mathbf{x}_k}{|\mathbf{x}_j - \mathbf{x}_k|^2 + \epsilon^2},$$

where  $\mathbf{x}_j$  is a two dimensional vector,  $Q_j^2$ ,  $\nu$ , and  $\alpha$  are diagonal 2 by 2 matrices,  $\epsilon$  is a smoothing parameter, and  $C_{sc}$  parameterizes the strength of the space charge force. Each  $Q_j^2$  is different and chosen from a parabolic distribution.

Simulations were done by increasing  $N$  with a fixed integration time until results converged. For  $C_{sc} = 0$ , the simulations agree with the coasting beam dispersion relation within a few percent. Simulations with space charge are compared with the analytic theory in Fig. 9. With no spread in  $Q_j$  the tune shift is  $\Delta Q_0$ . Stable simulations of a smooth beam are green crosses and the red are unstable. The red threshold curve is calculated using linear space charge. The blue threshold curve is a hand estimate based on the soft upper limit discussed in [50]. The simulations show a much smaller effect than the hand estimate and the difference corresponds to a factor  $\sim 4$  in RF voltage. The resolution of this problem is a serious, practical matter. Accurate determinations of required momentum aperture and RF voltage could result in significant cost savings for future machines.

## 5 ACKNOWLEDGEMENTS

This work has benefited from conversations with P. Channell, V.A. Danilov, R. Davidson, W. Fischer, M. Furman,

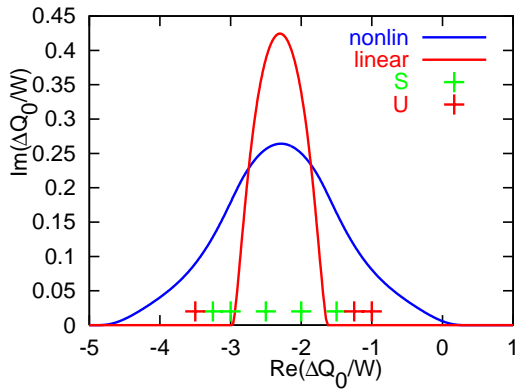


Figure 9: Various estimates of nonlinear space charge effects with  $P(Q) = (3/4W)(1 - (Q - Q_0)^2/W^2)$ .

K. Harkay, G. Lambertson, Y.Y. Lee, R.J. Macek, M. Pivi, A.G. Ruggiero, H. Qin, T.S. Wang, J. Wei and S.Y. Zhang. Special thanks to the BNL vacuum group for preparing the titanium nitride coated samples and the CERN vacuum group for measuring the secondary yield.

## 6 REFERENCES

- [1] G.I. Budker, G.I. Dimov, V.G. Dudnikov, *Proceedings of the International Symposium on Electron and Positron Storage Rings*, VIII-6-1, Saclay 1966.
- [2] G.I. Budker, G.I. Dimov, V.G. Dudnikov, A.A. Sokolov, V.G. Shamovskiy, *Sixth International Conference on High Energy Accelerators*, A-103, Cambridge Massachusetts, 1967.
- [3] V. Dudnikov, 8th ICFA Beam Dynamics Mini-workshop, Santa Fe, (2000), available online at <http://www.aps.anl.gov/conferences/icfa/two-stream.html>
- [4] H. G. Hereward, CERN 71-15 (1971).
- [5] E. Keil, B. Zotter, CERN/ISR-TH/71-58, (1971).
- [6] D. Neuffer, E. Colton, D. Fitzgerald, T. Hardek, R. Hutson, R. Macek, M. Plum, H. Thiessen, T.S. Wang *NIM A* **321** p1 (1992).
- [7] M. A. Plum, D.H. Fitzgerald, D. Johnson, J. Langenbrunner, R.J. Macek, F. Merrill, P. Morton, B. Prichard, O. Sander, M. Shulze, H.A. Thiessen, T.S. Wang, C.A. Wilkinson, PAC97 p 1611.
- [8] R. Macek, AIP Conf. 448, p116, (1998)
- [9] G. Arduini, V. Baglin, O. Bruning, R. Cappi, F. Caspers, P. Collier, I.R. Collins, K. Cornelis, R. Garoby, O. Gröbner, B. Henrist, N. Hilleret, W. Hofle, J.M. Jimenez, J.M. Laurent, T. Linnekar, E. Mercier, M. Pivi, F. Ruggiero, G. Rumolo, C. Scheuerlein, J. Tuckmantel, L. Vos, F. Zimmermann EPAC00, p259, (2000) and references therein.
- [10] R. Cappi, M. Giovannozzi, E. Metral, G. Metral, F. Zimmermann, PAC01, p682 (2001).
- [11] R. Cappi, M. Giovannozzi, E. Metral, G. Metral, G. Rumolo, F. Zimmermann, PRSTAB, **5**, 094401, (2002)
- [12] W. Fischer *etal* EPAC02, 1485, (2002)
- [13] H.C. Hseuh, L.A. Smart, S.Y. Zhang, EPAC02, 2559, (2002)
- [14] W. Fischer, J.M. Brennan, M. Blaskiewicz, T. Satogata, PRSTAB **5**, 124401, (2002).
- [15] M. Blaskiewicz, AIP Conf. 496, p321, (1999).
- [16] M. Blaskiewicz, M.A. Furman, M. Pivi, R.J. Macek, PRSTAB, **6** 104203 2003
- [17] K. Ohmi, T. Toyama, C. Ohmori, PRSTAB **5**, 114402, (2002).
- [18] G.V. Stupakov, LHC Project Report 141 (1997).
- [19] M.A. Furman and G. Lambertson, in Proceedings of the International Workshop on Multibunch Instabilities in Future Electron and Positron Colliders, Tsukuba, Japan, 1997.
- [20] O. Gröbner, PAC97
- [21] F. Zimmermann, PAC01, p666, (2001).
- [22] M. Plum, PSR Tech Note PSR-94-001 (1994).
- [23] V. Danilov, J. Galambos, D. Jeon, J. Holmes, D. Olsen, D. Fitzgerald, R. Macek, M. Plum, J. Griffin, A. Burov, PAC99, p1201 (1999).
- [24] P. Thieberger, A.L. Hanson, D.B. Stetski, V. Zajic, S.Y. Zhang, H. Ludewig, PRA, **61**, 042901 (2000).
- [25] M. Pivi, M.A. Furman *Phys Rev S.T Accel Beams*, **5** 124404
- [26] U. Iriso-Ariz *etal*, these proceedings
- [27] S.Y. Zhang *etal*, these proceedings
- [28] B. Henrist, N. Hilleret, C. Scheuerlein, M. Taborelli, G. Vorlaufer, EPAC02, p2553 (2002).
- [29] Y. Kijima, S. Mitsunobu, T. Furuya, R. Noer, The 10th Workshop on RF Superconductivity, contribution PT027, available online at <http://conference.kek.jp/SRF2001/>.
- [30] R. Macek, 8th ICFA Beam Dynamics Mini-workshop, Santa Fe, (2000), available online at <http://www.aps.anl.gov/conferences/icfa/two-stream.html>
- [31] R.J. Macek, PAC01 p688 (2001).
- [32] R.J. Macek Proceedings ICANS XV, KEK Nov 2001, p229.
- [33] A. Browman, 8th ICFA Beam Dynamics Mini-workshop, Santa Fe, (2000).
- [34] K. Ohmi, F. Zimmermann, E. Perevedentsev, *Phys Rev E*, **65** 016502 (2001).
- [35] E. Perevedentsev, CERN-2002-001, p 171. (2002).
- [36] Y. Chin, CERN/LEP-TH/88-05 (1988), and references therein.
- [37] K. Ohmi, PRL, **75**, 1526 (1995).
- [38] K. Ohmi, F. Zimmermann, PRL, **85** 18, p3821, (2000).
- [39] G. Rumolo, F. Zimmermann, H. Fukuma, K. Ohmi, PAC01, p1889, (2001).
- [40] B.V. Chirikov, *Sov. Atomic Energy*, **19** p1149 (1965).
- [41] L. J. Laslett, A. M. Sessler, D. Möhl, NIMA, **121**, p517, 1974.
- [42] R. C. Davidson, H. Qin, P. H. Stoltz, *Phys Rev ST Accel Beams*, 054401, 1999.
- [43] T.S.F. Wang, P.J. Channell, R.J. Macek, R. Davidson, *Phys Rev S.T Accel Beams*, **6** 014204 (2003).
- [44] P.J. Channell, *Phys Rev S.T Accel Beams* **5** 114401 (2002).
- [45] M. Blaskiewicz, 8th ICFA Beam Dynamics Mini-workshop, Santa Fe, (2000).
- [46] T.S. Wang, P.J. Channell, R. Macek, R.C. Davidson, PAC01, 704, (2001)
- [47] R.C. Davidson, H. Qin, P.J. Channell, PRSTAB, **2** 074401 (1999).
- [48] H. Qin, R.C. Davidson, E. Startsev, W.W. Lee, PAC01, 693, (2001)
- [49] H. Qin, E. Startsev, R.C. Davidson, PRSTAB **6** 014401 (2003)
- [50] M. Blaskiewicz, *Phys Rev ST Accel Beams* **4**, 044202, (2001).